ISSN 1392–1207. MECHANIKA. 2015 Volume 21(4): 313–322

A milling deformation model for aluminum alloy frame-shaped workpieces caused by residual stress

Yuan Haiyang*''***, Wu Yunxin*'**, Gong Hai*'**, Wang Xiaoyan*'****
**School of Mechanical and Electrical Engineering, Central South University, Changsha 410083, China*
***State Key Laboratory of High Performance Complicated Manufacturing, Central South University, Changsha, 410083 China*
****Hunnan College of Information, Changsha, 410083 China*

crossref http://dx.doi.org/10.5755/j01.mech.21.3.9176

1. Introduction

With the development of aerospace manufacturing, high-performance aluminum alloy with high strength, high toughness and corrosion resistance is indispensable [1-2]. Thin-walled workpieces have been widely used, such as the overall frame, the whole beam, the whole wall plate, etc, but the integral components with large size, complicated structure, thin wall, high precision features require high standard of manufacturing techniques. Materials removal makes its rigidity change and causes deformation. According to the existing researches [3-4], BI Yunbo et al. [3] considered that the milling deformation of the overall structure is mainly caused by the initial residual stress, CHENG and Qun-lin et al. [4] suggested that the asymmetry and unreasonable process technology of parts is another reason of milling deformation. The deformation after milling is far beyond the assembly range of permission error, and correction procedures are needed in order to satisfy requirement. These operations not only reduce productivity, but also increase the parts' scrap, bring huge economic loss to manufacturers [5].

In view of the milling deformation, researchers have carried out substantial work on both simulation and experiment. Keith A. Young studied the thin-walled parts' machining stress and the deformation. He also used the combination function to fit the machining stress [6]. Guo H. has established finite element and experimental models to forecast aluminum alloy thin-walled milling deformation [7]. Shang studied the structure stability of processing components caused by initial residual stress and discussed residual stress distribution of the whole layer stripping artifacts [8]. He Ning proposed control strategy of the deformation of thin-walled parts by using finite element analysis method [9]. Weinert K. et al. studied the workpiece deformations and shape deviations caused by cutting heat using finite element analysis method and experiment method [10-11]. Tang Aijun and Liu Zhanqiang proposed a new analytical deformation model suitable for static deformations prediction of thin-walled plate with low rigidity [12].

However, the majority of previous research works in deformations have mainly focused on sample thin-walled workpieces based on the experimental and finite element analysis. The deformation of simple aluminum alloy parts can be worked out using these methods, but the process is complex and time-consuming. This paper presents an empirical model for the deformations of aluminum alloy frame-shaped workpieces as a function of residual stress, milling rates, workpieces length and workpieces width. This model was built based on the elastic theory, finite element simulation and experimental test and can improve calculation accuracy and expedite calculation speed in the aluminum alloy frame-shaped workpieces milling deformations calculation.

2. Milling deformation forecast model for whole layer stripping piece

2.1. Modeling of milling deformation for whole layer stripping piece

Aluminum alloy parts usually made from aluminum alloy thick plates. The residual stress in aluminum alloy thick plates is large and assumed to be varied from thickness only [13]. The stress distribution through thickness direction is shown in Fig. 1.

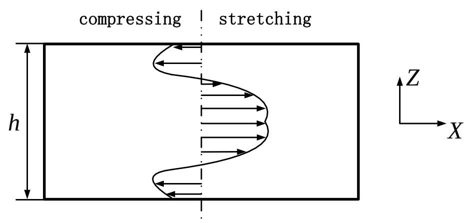

Fig. 1 The residual stress distribution of aluminum alloy plate

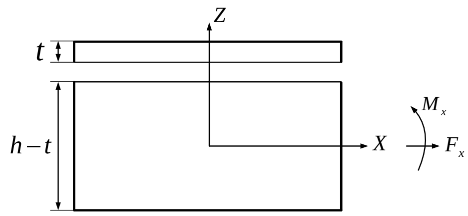

Fig. 2 Layer removal method schematic

Fig. 2 shows the process of layer removal, axis X stands for length direction of plate, Y stands for the width direction and Z stands for thickness direction in this paper. After one layer material removed, residual stress in this layer was released and the residual stress in aluminum alloy thick plate will be redistributed, leading to the deformation of remaining component. According to mechanics of materials [14], the strains (as in show in Fig. 3) and stresses in the plate can be described as Eqs. (1) and (2).

$$\begin{cases}\varepsilon_x = \varepsilon_{x0} + z\rho_x; \\ \varepsilon_y = \varepsilon_{y0} + z\rho_y. \end{cases} \tag{1}$$

The origin of axis z locates at $(h-t)/2$; ε_{x0} and ε_{y0} stand for strains in x and y directions at $z = 0$ respectively, ρ_x and ρ_y stand for curvatures of the plate in x and y directions. Thus σ_x and σ_y can be expressed as:

$$\begin{cases}\sigma_x = E'\left(\varepsilon_x + \mu\varepsilon_y\right); \\ \sigma_y = E'\left(\varepsilon_y + \mu\varepsilon_x\right), \end{cases} \tag{2}$$

where $E' = E/(1 - \mu^2)$, E is elastic modulus, and μ is poisson's ratio. When the surface layer of thickness t is removed, the internal forces in Xdirection F_x internal forces in Ydirection F_y , internal moment in X direction M_x and internal moment in Ydirection M_y are unbalanced, which can be denoted as:

$$\begin{cases} F_x = \int_{-\frac{h-t}{2}}^{\frac{h-t}{2}} \sigma_x(z)dz; & M_x = \int_{-\frac{h-t}{2}}^{\frac{h-t}{2}} \sigma_x(z)zdz; \\ F_y = \int_{-\frac{h-t}{2}}^{\frac{h-t}{2}} \sigma_y(z)dz; & M_y = \int_{-\frac{h-t}{2}}^{\frac{h-t}{2}} \sigma_y(z)zdz, \end{cases} \tag{3}$$

where $\sigma_x(z)$ and $\sigma_y(z)$ stand for stresses in x and y directions at z respectively. When thickness t of the removed layer inclines to zero, $\sigma_x(z)$ and $\sigma_y(z)$ can be substituted by average stresses of this layer. σ_{x1} and σ_{y1} represent the average stresses in x and y directions of first layer, while σ_{xn} and σ_{yn} reprent the average stresses of the n-th layer. When the first layer is removed, Eq. (3) can be simplified to:

$$\begin{Bmatrix} F_x \\ F_y \\ M_x \\ M_y \end{Bmatrix} = \begin{Bmatrix} t\sigma_{x1} \\ t\sigma_{y1} \\ \frac{1}{2}ht\sigma_{x1} \\ \frac{1}{2}ht\sigma_{y1} \end{Bmatrix}. \tag{4}$$

Due to the compressive stress releasing of first layer, remaining components will be bending, which is shown in Fig. 3.

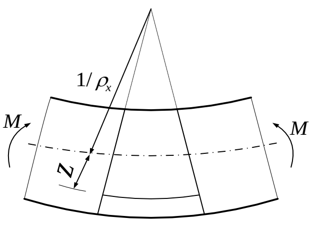

Fig. 3 Deformation pattern after layer removal

From Eqs.(1)-(4), strains ε_{x0} and ε_{y0} along with curvatures ρ_x and ρ_y can be deduced as:

$$\left.\begin{aligned} \begin{Bmatrix}\varepsilon_{x0} \\ \varepsilon_{y0}\end{Bmatrix} &= \frac{t}{E'(h-t)}\begin{bmatrix} 1 & -v \\ -v & 1 \end{bmatrix}\begin{Bmatrix}\sigma_{x1} \\ \sigma_{y1}\end{Bmatrix}; \\ \begin{Bmatrix}\rho_x \\ \rho_y\end{Bmatrix} &= \frac{6ht}{E'(h-t)^3}\begin{bmatrix} 1 & -v \\ -v & 1 \end{bmatrix}\begin{Bmatrix}\sigma_{x1} \\ \sigma_{y1}\end{Bmatrix}, \end{aligned}\right\} \tag{5}$$

where, ρ_{x1} and ρ_{y1} are curvature of component when the first layer has been removed. When the second layer is removed, ρ_{x1} and ρ_{y1} are induced by the combination effect of stresses σ_{x1} and σ_{y1} in the first layer and stresses σ_{x2} and σ_{y2} in the second layer. Similarly, while the n-th layer is removed, ρ_{xn} and ρ_{yn} are induced by the combination effect of stress in the n^{th} layer and stress in the $(n$-1)-th layers, which can be denoted as a matrix:

$$\begin{bmatrix} c_{11} & 0 & \cdots & 0 \\ c_{12} & c_{22} & 0 & 0 \\ \vdots & \vdots & \vdots & 0 \\ c_{1n} & c_{2n} & \cdots & c_{nn} \end{bmatrix}\begin{bmatrix} \sigma_{x1} & \sigma_{y1} \\ \sigma_{x2} & \sigma_{y2} \\ \vdots & \vdots \\ \sigma_{xn} & \sigma_{yn} \end{bmatrix} = \begin{bmatrix} \rho_{x1}+\mu\rho_{y1} & \rho_{y1}+\mu\rho_{x1} \\ \rho_{x2}+\mu\rho_{y2} & \rho_{y2}+\mu\rho_{x2} \\ \vdots & \vdots \\ \rho_{xn}+\mu\rho_{yn} & \rho_{yn}+\mu\rho_{xn} \end{bmatrix}, \tag{6}$$

where $c_{ij} = -\dfrac{6t[h+(j-2i+1)t]}{E'(h-jt)^3}$ $(j = 1,2,3\cdots n \quad i \le j)$.

If the residual stress is known, the curvature ρ_{xn} and ρ_{yn} can be calculated by Eq. (6), which can be denoted as a matrix:

$$\begin{aligned} \begin{bmatrix} \rho_{x1} & \rho_{y1} \\ \rho_{x2} & \rho_{y2} \\ \vdots & \vdots \\ \rho_{xn} & \rho_{yn} \end{bmatrix} &= \frac{1}{1-\mu^2}\begin{bmatrix} c_{11} & 0 & \cdots & 0 \\ c_{12} & c_{22} & 0 & 0 \\ \vdots & \vdots & \vdots & 0 \\ c_{1n} & c_{2n} & \cdots & c_{nn} \end{bmatrix} \times \\ &\times \begin{bmatrix} \sigma_{x1} & \sigma_{y1} \\ \sigma_{x2} & \sigma_{y2} \\ \vdots & \vdots \\ \sigma_{xn} & \sigma_{yn} \end{bmatrix}\begin{bmatrix} 1 & -\mu \\ -\mu & 1 \end{bmatrix}. \end{aligned} \tag{7}$$

Using Eq. (7), the bend deformation curvature of whole layer stripping piece can be calculated no matter how many layers are triped. However, it is difficult to evaluate amount of deformation when the bend deformation curvatures are known. So the amount of bend deformation Δd (the bottom displacement of artifact along axis z is used to evaluate bend deformation. The definition of Δd is shown in Fig. 4. When bend deformation is little, circle length CD is equal to straight length. Based on the geometry situation and Pythagorean Theorem, Eq. (8) can be got:

$$\left(\frac{1}{\rho}\right)^2 - \left(\frac{1}{\rho} - \Delta d\right)^2 = \left(\frac{L}{2}\right)^2 - \left(\Delta d\right)^2. \tag{8}$$

So the relationship of curvature and deflection can be deduced as:

$$\Delta d = \frac{\rho L^2}{8} \tag{9}$$

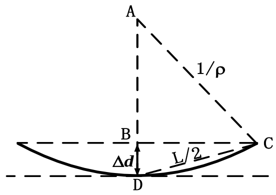

Fig. 4 The relationship of curvature and deflection

2.2. Comparing the forecast model result and simulation result

The deformation of whole layer stripping piece was simulated by models on MSC.MARC [15]. The size of plate is 100 mm × 100 mm × 20 mm, elastic modulus $E = 71$ GPa and Poisson ratio $\mu = 0.33$ and residual stress is shown in Fig. 5. Hexahedral element mesh was used to control the number of milling layer, and the method of killing or activating elements was used to simulate milling. Along the thickness direction, part was divided into eight steps. Residual stress which satisfies force and moment equilibrium was loaded into each unit of model.

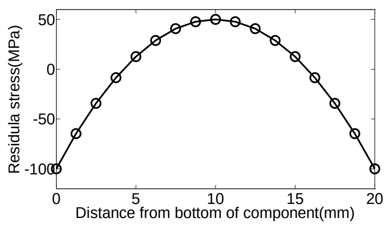

Fig. 5 The distribution of residual stress along the thickness direction

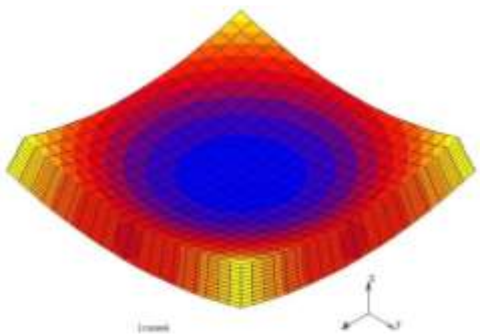

Fig. 6 The deformation nephogram of artifact after layer removal（enlarged view）

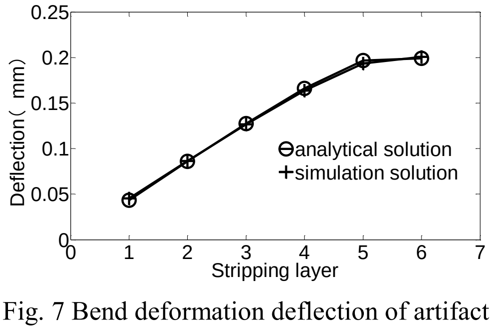

Fig. 7 Bend deformation deflection of artifact

The bottom displacement of artifact along axis z on the length direction was deduced from FEM (as is shown in Fig. 6) and bend deformation Eqs. (7) and (9) respectively. Results are shown in Fig. 7 and it indicate that the simulation values of deformation were close to the analytical values after milling, so the accuracies of bend deformation Eqs. (7) and (9) are verified when aluminum alloy plate is milled into the whole layer stripping piece.

3. Milling deformation forecast model for frame-shaped parts

In the actual production, aluminum alloy plates usually milled into box-parts. The whole layer stripping pieces and frame-shaped component are made from thick plates that with the same Level and distribution of initial residual stress. So the deformation of frame-shaped component cause by residual stress is similar with that of whole layer stripping pieces. The FEM result (as is shown in Fig. 8) proves that box-parts appear bend deformation as the same as whole layer stripping piece. The diference is that the bend deformation curvature ρ^* of box-parts is smaller than the bend deformation curvature ρ of whole layer stripping plate due to its larger bending rigidity. So when the bend deformation curvature ρ of whole layer stripping pieces were calculated by Eq. (7), the bend deformation curvature ρ^* of box-parts can be got if the relationships between ρ and ρ^* are knew. In order to find out these relationships, FEM of frame-shaped components are done as follow.

a

b

Fig. 8 The deformation schematic: a - The whole layer stripping piece; b - box-parts

3.1. Finite element analysis of frame-shaped component

The difference between whole layer stripping pieces and frame-shaped component is that they have different mill rate in horizontal direction and different slot number. So their influences on deformation were studied by FEM method.

3.1.1. Influence of milling rate

Milling depth of frame slot in the same component is assumed to be consistent. Definition of milling rate is shown in Fig. 9 (in milling directions), the width direction milling rate represent material removal percentage in Y direction while the length direction milling rate represent material removal percentage in X direction. X, Y, Z direction represent the length, width and heigth direction of box-part respectively. The size of plate is 2000 mm × 600 mm × 40 mm. The material parameters, the way of element mesh generation and milling simulation are the same as that in section 2.2. Along the thickness direction, part was divided into 16 steps. The residual stresses are the same as that in experimental and are shown in Fig. 10.

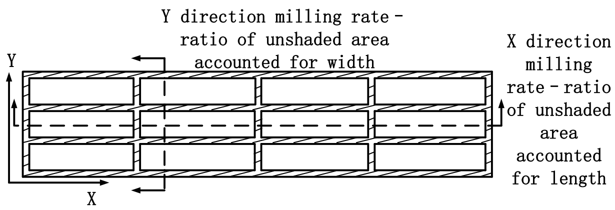

Fig. 9 Definition of milling rate

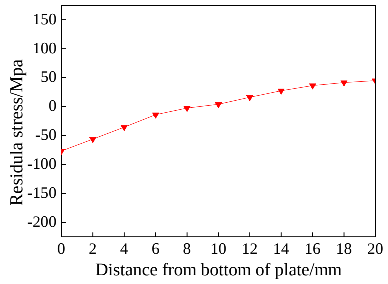

a

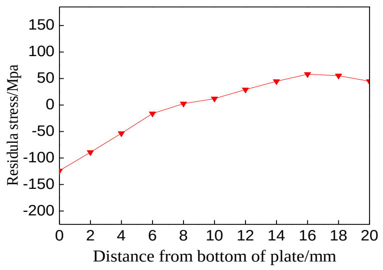

b

Fig. 10 Residual stress of aluminum alloy plate: a - rolling direction stress; b - Transversal stress

3.1.1.1. Influence of milling rates in width direction (Y direction)

The FEM models are milled into frame components whose wall thickness are 20 mm and bottom thickness is 30 mm. The width milling rates are varied through changing the thickness of length direction rib, but length milling rates are 98%. The value of width milling rates 93.33%, 90%, 86.67%, 83.33%, 80%, 76.67%, 66.67%. The simulation results are shown in Fig. 11. The black curve represents bend deflection in length direction, while the red one represents bend deflection in width direction. It can be seen that length direction bend deflection increase with rising width milling rate, but the changes of width are inconspicuous.

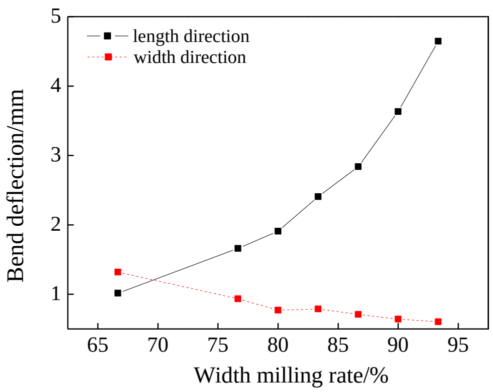

Fig. 11 The effect of width milling rate on the deformation

So a conclusion that the width direction milling rate mainly affect the bend deformation in length direction and has little effect on the width direction bend deformation can be deduced from the simulation results.

3.1.1.2. Influence of milling rates in length direction (X direction)

Three models have been milled into frame components whose wall thickness are 20mm and bottom thickness is 30 mm. Their width milling rates are 90%, but length milling rates are 95%, 96%, 98% respectively. Their length milling rates are varied through changing the thickness of width direction rib. Fig. 12 shows that bend deformations in length direction at the bottom are essentially uniform, but different in width direction.

So a conclusion that the length direction milling rate mainly affect the bend deformation in width direction and has little effect on the length direction bend deformation can be obtained from the simulation results.

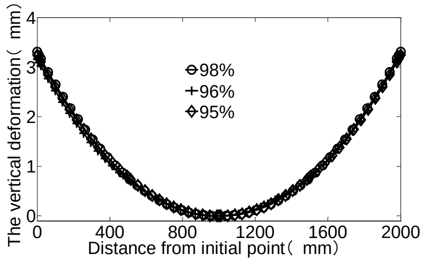

a

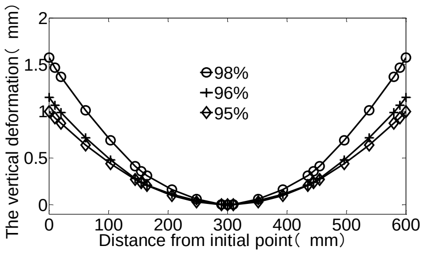

b

Fig. 12 Bend deformation under different length milling rate: a - Length bend deformation; b - Width bend deformation

3.1.1.3. Influence of milling rates in height direction (Z direction)

The model is equally divided into twenty steps along the thickness direction and milled into single frame components with wall thickness 10 mm. Milling depth increases from 2 mm to 38 mm, then bottom bend deformations under different heigth milling rate were deduced as shown in Fig. 13. From Fig. 13 it can be knew that length bend deformation increases then decreases following the increasing of milling depth. It reached the peak when heigth milling rate is approximately 40% and keeping at the same level when milling rate is between 75% and 95%. Width bend deformation increases until milling rate reaches 75%, then drops.

So based on the simulation results a conclusion that the height direction milling rate not only affect the bend deformation in length direction but also affect the width direction bend deformation can be obtained.

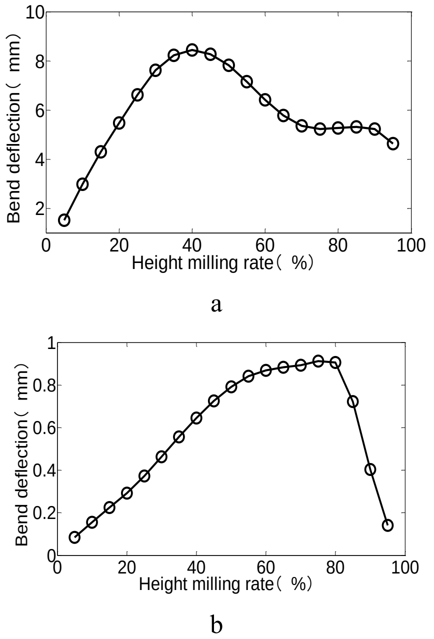

Fig. 13 Deformation changes following milling depth: a - Length direction; b - Width direction

3.1.2. Influence of milling slot number

Plates have been milled into single frame components whose length direction milling rates are 98%, milling depth is 30 mm and width milling rates are different. While corresponding non-single frame components with the same width and length milling rate but different slot number. Simulation results are shown in Table 1.

Table 1

Deformation comparison between single frame and several frames

u_y, %	Single	Non-single		Error
	deformation, mm	Slot number	deformation, mm	
96.67	5.4521	3	5.4216	-1.27%
95	4.9394	2	4.9102	-0.59%
93.33	4.5541	3	4.5069	-1.04%
91.67	4.2418	4	4.2461	0.10%
90	3.9768	2	3.9901	0.33%
86.67	3.5421	3	3.5494	0.21%
83.33	3.1603	4	3.3093	4.71%
80	2.8787	5	3.0317	5.32%

Table 1 shows, the slot number has litter effect on deformation when milling rate is greater than 80%, so it is reasonable to just consider the effect of milling rate in the calculation of bend deformation.

3.2. Modeling of milling deformation for frame-shaped component

Using u_x, u_y, u_z represent milling rates of box-part in X (length direction), Y (width direction) and Z (heigth direction) direction. According to the analysis in section 3.1, it can be got that the bend deformation in x direction is mainly affected by y and z direction milling rate while the bend deformation in y direction is mainly affected by x and z direction milling rate. So $k_x(u_y,u_z)$ and $k_y(u_x,u_z)$ are asumed to be correction factor functions corresponding the affect of stiffeners. For plates and box-parts with the same Z direction milling rate but diffrernt X and Y direction milling rates (for plates X and Y direction milling rates are 100%), if the bend deformation curvatures ρ_x and ρ_y (equal to ρ_{xn} and ρ_{yn} in Eq. (7)) of whole layer stripping plate are calculated using Eq. (7), the bend deformation curvatures ρ^*_x and ρ^*_y (equal to ρ^*_{xn} and ρ^*_{yn} in Eq. (7)) of box-part can be calculated as follow:

$$\rho_x^* = k_x\left(u_y, u_z\right)\rho_x; \quad \rho_y^* = k_y\left(u_x, u_z\right)\rho_y, \tag{10}$$

where, ρ^*_x and ρ^*_y stand for bend deformation curvature of box-parts in X and Y direction respectively, ρ_x and ρ_y stand for bend deformation curvature of whole layer stripping piece in X and Y direction.

From Eqs. (9) and (10), the deflection can be deduced as:

$$\Delta d_x = \frac{\rho^*_x L_x^2}{8}; \ \Delta d_y = \frac{\rho^*_y L_y^2}{8}, \tag{11}$$

where, Δd_x and Δd_y are x and y direction deformation deflection when milling rate in x, y and z direction are u_x, u_y and u_z.

3.3. The determination of curvature correction function in milling deformation model

Most of the box components are thin-walled workpieces, and they are milled from rectangular aluminum plate. According to the results of above analysis and actual production situation, their length bend deformation is greater than width if the workpiece length is far greater than workpiece width and the deformation of parts can be represented by the deformation in length direction. So the length bend deformation is mainly discussed in this paper, while width bend deformation is ignored.

ρ_x and ρ_y in Eq. (8) can be calculated from Eq. (7), ρ^*_x and ρ^*_y can be obtained from FEM results. Then the valve of $k_x(u_y, u_z)$ and $k_y(u_x, u_z)$ can be deduced from Eq. (10) when ρ_x, ρ_y, ρ^*_x and ρ^*_y are knew. A great number of correction factors k_y with different u_x and u_z were calculated using this method. The results are shown in Figs. 14-16. From Fig. 14, it can be got that under the same width milling rate, when height milling rate increase, correction factors decrease then increase. In Fig. 16, under the same height milling rate, correction factors increases with increasing width milling rate. The relation among width milling rate, height milling rate and correction factor is shown in Fig. 16.

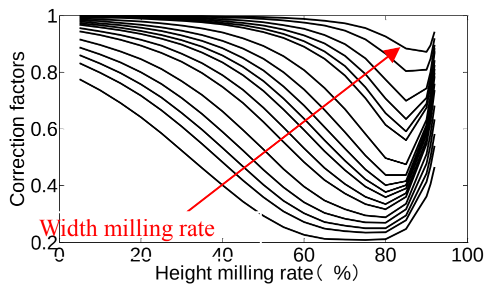

Fig. 14 The changes of correction factors following with height milling rate

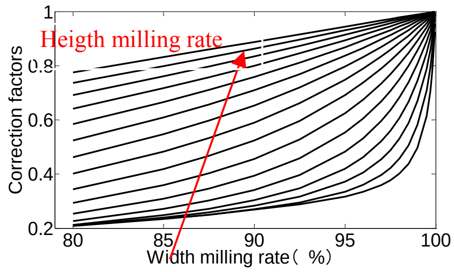

Fig. 15 The changes of correction factors following with width milling rate

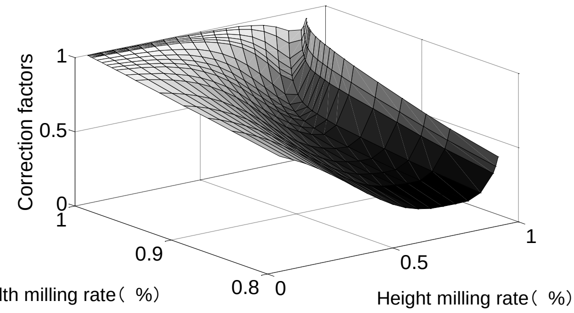

Fig. 16 Fitting of correction factors

These correction factors were multivariate regressive analyzed using matlab program, and the correction function regression equation was given out as:

$$k_x(u_y,u_z)=\frac{-18.1823+57.1136\,ln u_z+70.2911u_y+27.6109\,ln^2 u_z-50.8324{u_y}^2-45.7804u_y ln u_z}{1-11.5282\,ln u_z+50.5598u_y+27.8709\,ln^2 u_z-50.2374{u_y}^2+23.1081u_y ln u_z} \quad (12)$$

The root mean square error of this regression equation is 0.006935. Plug $k_x(u_y, u_z)$ into Eq. (10) the bend deformation curvature ρ^*_x of box-parts in X direction can be obtained if the bend deformation curvature ρ_x of whole layer stripping piece was obtained from Eq. (7), then the amount of bend deformation Δd_x can be worked out using Eq. (11).Using the same method $k_y(u_x, u_z)$, ρ^*_y and Δd_y also can be got.

4. Experiment of milling deformation

4.1. Preparation of experiment

The experimental material, 7075 aluminum alloy plate with dimension 1200 mm × 230 mm × 40 mm, the elastic modulus $E = 71$ GPa and Poisson ratio $\mu = 0.33$. After solution heat treatment the plate was immerging quenched in 20°C water, processed with pre-stretching of 1%. The residual stresses are tested by Proto iXRD diffraction device (show in Fig. 17) and the method proposed by gong-hai [12]. The distribution of residual stress is shown in Fig. 9. The measurement precision of iXRD diffraction device is ±10 MPa .As is show in Fig. 9, the average rolling stress is -65.7 MPa and traverse stress is -114.8 MPa. Then three specimens with dimension 450 mm × 112 mm × 40 mm were cut from the pre-stretched plate, their numbers are A#, B#, C# respectively and their geometry size after mill are shown in Fig. 18. A# and B# products have the same length milling rate and width milling rate, different number of rib along length direction, while B# and C# products with the same number of rib along length direction and width milling rate, different number of rib along width direction and length milling rate. Three specimens were milled by XKN714 milling machine following the milling parameters shown in Table 2, picture of real products after milled is shown in Fig. 19.

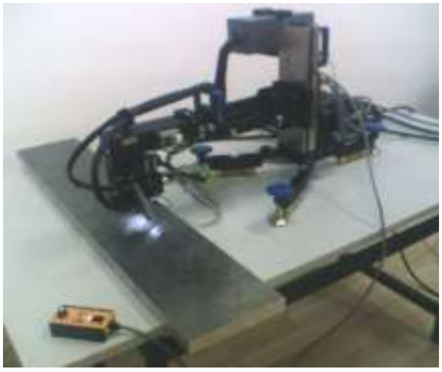

Fig. 17 iXRD diffraction device

Table 2

Milling parameters

Number of plate	A#	B#	C#
material of cutter	tool steels		
Diameter of cutter	20 mm		
Milling depth	30 mm		
speed of main spindle	200 r/min		
feed speed	200 mm/min		
way of milling	Outer-ring milling type		
type of components	Single-box	Double-box	Four-box
Wall and rib thickness (length)	6 mm	4 mm	4 mm
Wall and rib thickness (width)	10 mm	10 mm	10 mm

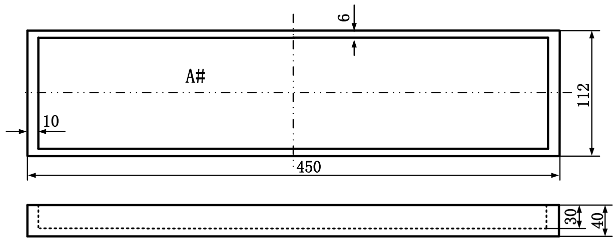

a

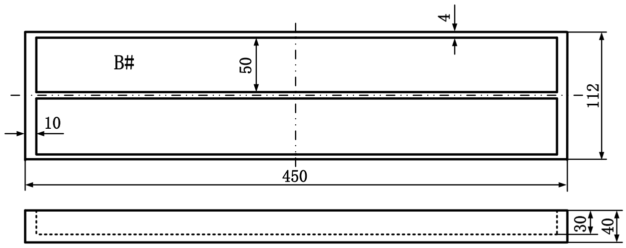

b

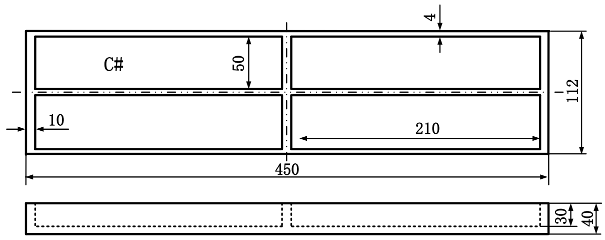

c

Fig. 18 Machining of the parts diagram

Fig. 19 Picture of real products after milled

4.2. Experimental results and analysis

As is shown in Fig. 19, the centerlines in length direction and width direction (line A and line B) of component bottom are selected to analysis deformation of parts in length and width direction. The deformation measure points are shown in Fig. 20 and axis z displacement of low-water mark in bottom is set to zero. Coordinate geometry of centerlines before and after milling are measured by Global Status575 type three-coordinates measuring instrument (as show in Fig. 21) the measuring accuracy of which is $0.3 + L/1000$ [μm]. Deflections can be determined by subtracting coordinate values before milling from the coordinate values after milling. The results are show in Figs. 22-24.

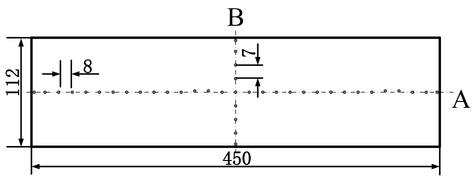

Fig. 20 Deformation measure point (bottom of part)

Fig. 21 Three-coordinates measuring instrument

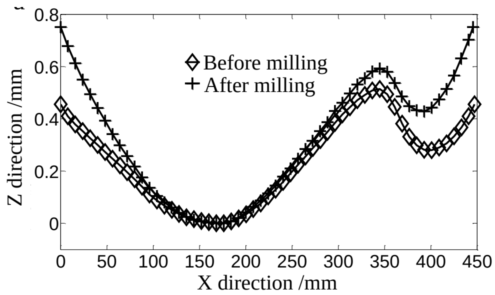

a

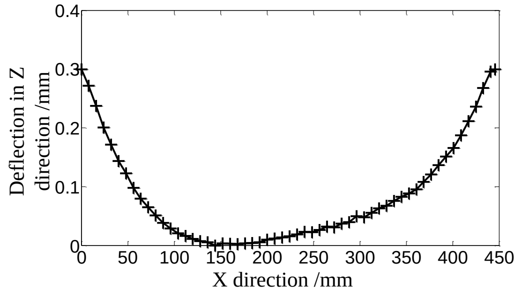

b

Fig. 22 Bend deformations in length direction of A# sample: a - measuring result; b - amount of deformation

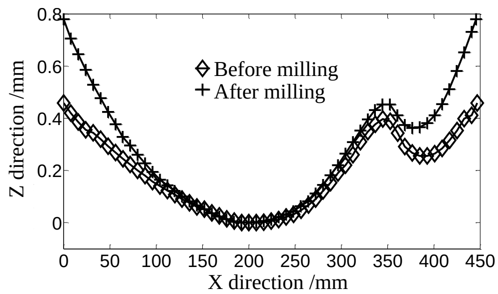

a

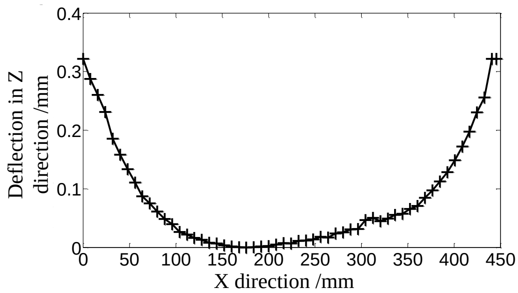

b

Fig. 23 Bend deformations in length direction of B# sample: a - measuring result; b - amount of deformation

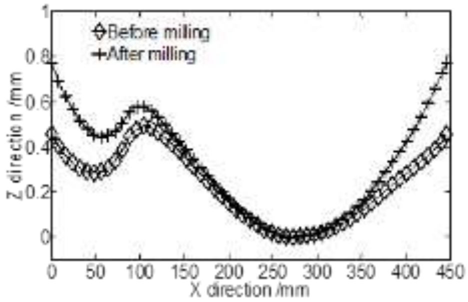

a

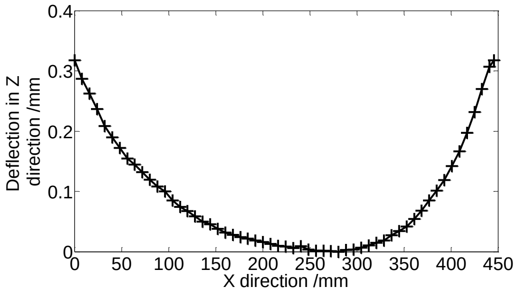

b

Fig. 24 Bend deformations in length direction of C# sample: a - measuring result; b - amount of deformation

From the results in Fig. 22-24 it can be got that deformations in length direction of A#, B# and C# are 0.31536 mm, 0.32199 mm and 0.336883 mm. The width direction deformation of three parts, which are not shown in figures, also can be got by this method. Deformations in width direction of A#, B# and C# are 0.03281 mm, 0.03405 mm and 0.02404 mm. Discrepancy of bend deformation deflection in length direction of A# and B# is 2.06% and width direction is 3.64%. Discrepancy of bend deformation deflection in length direction of B# and C# is 4.42% and width direction is 29.4%.

A#, B# and C# products have the same width milling rate, different number of rib and length milling rate. The deformations in length direction of three parts are almost equal. So a conclusion that the bend deformation in length direction are mainly affected by width milling rate and has little related to the number of rib and length direction milling rate can be deduced from the experiment results; A# and B# products have the same length milling rate and different number of rib, and their deformations in width direction are almost equal. B# and C# products have different length milling rate, and they have very different deformation in width direction. This indicate that the bend deformation in width direction are mainly affected by length milling rate.

These conclusions are agree well with that were proposed in section 3.1. It proved the correctness of the modeling method and simulation results.

4.3. Results comparison

As is shown in Fig. 17, dimension of workpieces are 450 mm × 112 mm × 40 mm, height milling rate is 75% and width milling rate is 89.29%. Parts before milling, average rolling stress is -65.7 MPa, traverse stress is -114.8 MPa and the distribution of residual stresses are showing in Fig. 9. If part is divided into 40 steps along height and 30 steps are moved during milling, then the length direction deformation curvature ρ_x of whole layer stripping piece can be deduced from Eq. (7) and the result is 5.6777×10^{-5} mm^{-1}. The correction factor $k_x(u_y, u_z)$ is 0.2539 can be deduced by plug width milling rate ($u_y = 89.29\%$) and height milling rate ($u_z = 75\%$) into Eq. (12). Using these results and the length of parts $L_x = 450$ mm, the bend deformation deflection of frame-shaped component is 0.3649 mm can be got from Eq. (11). The bend deformation of parts were calculated by simulation models using the same method mentioned in section 3 (models are shown in Fig. 25) and the results are shown in Table 3.

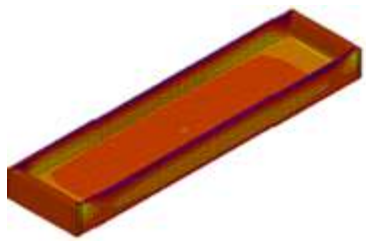

a

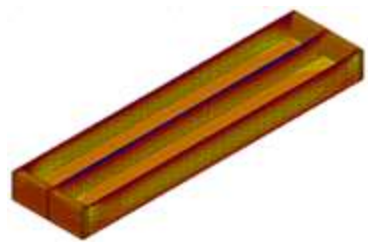

b

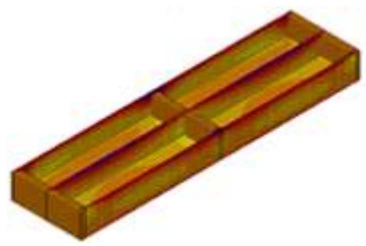

c

Fig. 25 Simulation models: a - sample A#; b - sample B#; c - sample C#

Table 3

Deformation results comparison

	forecasted result	A#		B#		C#	
		test result	simulation result	test result	simulation result	test result	simulation result
Deflection /mm	0.3649	0.31536	0.356887	0.32199	0.348111	0.336883	0.342883
Error /%	0	15.8%	2.20%	11.76%	4.6%	7.68%	6.03%

The results in Table 3 indicate that the forecasted result worked out from the milling deformation model agrees well with the test results and simulation results, and the biggest error is 15.8%. For each sample the deformation error between forecasted result and simulation result is significant bigger than that between forecasted result and test result. This is because this forecast model is deduced from simulation results and some other reasons that may affect the test results are not taking into account.

5. Conclusion

1. Milling deformation forecast model for whole layer stripping piece caused by residual stress was establashed using parsing method and the accuracy of the model was proved by simulation results.

2. The Milling deformation model of frame-shaped parts as a function of residual stress, milling rates and workpiece length was established. This model was composed by Eqs. (7), (10), (12) and (11) which can be used to calculate the milling deformation of frame-shaped parts caused by residual stress when the workpiece length is greater than four times of workpiece width. This model could easily work out the amount of deformation if the milling rates and residual stress were known. It has solved the problem that the milling deformation is difficult to predict.

3. The milling deformation forecast model and simulation model for frame-shaped parts were verified by experiment. The deformation results from the two methods agree well with the experimental results, and the largest error is 15.8% can meet the needs in engineering.

Acknowledgment

This work is funded by National Basic Research Program of China (Grant No. 2010CB731703).

References

1. **Palanivel, R; Koshy Mathews, P.; Murugan, N.** 2012. Development of mathematical model to predict the ultimate tensile strength of friction stir welded dissimilar aluminum alloy, Mechanika 18(5): 517-523. http://dx.doi.org/10.5755/j01.mech.18.5.2699.
2. **Kah, P.; Hiltunen, E.; Martikainen, J.; Katajisto, J.** 2009.Experimental investigation of welding of aluminum alloys profiles and wrought plate by FSW, Mechanika 79(5): 21-27.
3. **Cheng Qun-lin; Ke Ying-lin; et al.** 2006. Simulation of high-speed milling process of aerospace aluminum alloy, Journal of Zhejiang University (Engineering Science) 40(1): 113-117.
4. **Bi, Yun-bo; Ke, Ying-lin; et al.** 2008. Finite element simulation and analysis of deformation in machining of aeronautical aluminum alloy thin-walled workpiece, Journal of Zhejiang University (Engineering Science) 42(3): 397-402.
5. **Guo, Hun; Zuo, Dun-wen; et al.** 2008.Prediction of milling distortion for aero-thin-walled components, Journal of Jilin University (Engineering and Technology Edition) 38(1): 84-88.
6. **Keith A. Young** 2005. Machining-induced residual stress and distortion of thin parts, Washington University, USA.
7. **Guo, H; Zuo, D.W; et al.** 2009. Prediction on milling distortion for aero-multi-frame parts, Materials Science and Engineering 499(1-2): 230-233. http://dx.doi.org/10.1016/j.msea.2007.11.137.
8. **Shang Hyon shin** 1995. Prediction of the dimensional instability resulting from machining of residual stressed components, Texas Tech University, USA.
9. **He, Ning; Wang, Zhi-gang; Jiang, Cheng-yu; et al.** 2003. Finite element method analysis and control stratagem for machining deformation of thin-walled components, Journal of Materials Processing Technology 139(1): 332-336.
10. **Weinert, K; Biermann, D; Kersting, M; et al.** 2008. Experimental and computational analysis of machining processes for light-weight aluminum structures, Advanced Materials Research 43(1): 97-104. http://dx.doi.org/10.4028/www.scientific.net/AMR.43.97.
11. **Weinert, K; Grunert, S; Kersting, M.** 2006.Analysis of cutting technologies for lightweight frame components in flexible manufacture of lightweight frame structures, Advanced Materials Research 10(1): 121-132. http://dx.doi.org/10.4028/www.scientific.net/AMR.10.121.
12. **Tang Aijun; Liu Zhanqiang.** 2008. Deformations of thin-walled plate due to staticend milling force, Journal Of Materials Processing Technology 206: 345-351. http://dx.doi.org/10.1016/j.jmatprotec.2007.12.089
13. **Liao, Kai; Wu, Yun-xin; Gong, Hai; et al.** 2010. Prediction and measurement of quenching-prestretching stress in Aluminum Alloy Thick plate, The Chinese Journal of Nonferrous Metals 20(10): 1901-1906.
14. **Zhang, Shao-shi.** 2008. Newly organized mechanics of materials, China Machine Press，Beijing, 128-132.
15. **Chen Huo-hong.** 2007.New Marc finite element instance tutorial, China Machine Press, Beijing, 35-45.
16. **Gong Hai.** 2011. Research on Evolution and Evalution Model of Residual Stress in Aluminum Alloy Thick plate, Central South University.

Yuan Haiyang, Wu Yunxin, Gong Hai, Wang Xiaoyan

S u m m a r y

For the purpose to predict the machining distortion of aluminum alloy 7050 caused by residual stress, a milling deformation model of plate was built based on the elastic theory. The deformation of aluminum alloy plate with residual stress after whole layer milled was studied. On the basis of the amendment of the machining deformation prediction model of the plate, machining deformation model of aluminum alloy frame-shaped workpieces was established, which contains undetermined correction coefficients and evaluation parameter of milling deformation. In order to confirm the undetermined coefficients, several finite element models of the milling process of thick aluminum alloy plate were established by MSC. Marc software. The influences of the number of slots and milling rate on the milling deformation of thick aluminum alloy plate were analyzed. The FEM results show that correction coefficients mainly depend on milling rates when residual stress is constant. Equations of the correction coefficients were deduced by multivariate regressive analysis. Then the accuracy of this model was proved by experiment. The test results show that this model can accurately predict the machining deformation of aluminum alloy frame-shaped workpieces caused by residual stress and the largest error is 15.8%. This model provides guidanceto the calculation of the machining deformation of aluminum alloy frame-shaped workpieces.

Keyword: frame-shaped workpieces; finite element simulation; residual stress; milling deformation model.

Received January 09, 2015
Accepted May 27, 2015